Complex of alkylated derivative of 1,4-diazabicyclo[2.2.2]octane with palladium dichloride: synthesis, self-association, and biological activity

M. R. Ibatullina, E. P. Zhil′tsova,★ N. V. Kulik, A. P. Lyubina, S. K. Amerhanova, A. D. Voloshina, S. S. Lukashenko, N. Kh. Safina, and L. Ya. Zakharova

A. E. Arbuzov Institute of Organic and Physical Chemistry, Kazan Scientific Center of the Russian Academy of Sciences, 8 ul. Akad. Arbuzova, 420088 Kazan, Russian Federation. Fax: +7 (843) 273 2253. E-mail: Zhiltsova@iopc.ru

A new complex of 1-hexadecyl-4-aza-1-azoniabicyclo[2.2.2]octane bromide (cationic surfactant with a bicyclic head group) with palladium dichloride (1 : 1) was synthesized. The spectral properties of the metal complex, as well as the aggregation and solubilizing ability in DMSO—water mixture (50 : 50, v/v) were studied by IR and ^{1}H NMR spectroscopies, tensiometry, conductometry, potentiometry, dynamic and electrophoretic light scattering, and spectrophotometry (solubilization of hydrophobic dye Orange OT). It was found that the aggregation parameters and solubilizing activity of the system depend on the amphiphile content and on the colloidal state of the solution. High antimicrobial activity against Gram-positive (including antibiotic-resistant) strains, low hemolytic activity, and a reduced cytotoxic effect on the WI-38 normal human fetal lung cell line and the Chang liver normal human hepatocyte cell line was established.

Key words: alkylated derivative of 1,4-diazabicyclo[2.2.2]octane, metal complex, aggregation, solubilization, antimicrobial activity, hemolysis, cytotoxicity.

Natural or synthetic organometallic amphiphiles are important building blocks of supramolecular systems of different morphology.[1—5] Investigations of such systems represent an interdisciplinary research involving coordination chemistry, surface chemistry, biology, and materials science. The presence of a metal imparts the redox and magnetic properties to the surfactant, favors an increase in its charge,[6,7] and enhances the aggregation properties typical of conventional surfactants, as well as the solubilizing, catalytic, and biological activity.[8—13] This significantly extends the range of possible applications of surfactants and underlies the search for novel highly efficient specific-action or polyfunctional amphiphilic metal complexes.

Many original publications and reviews are devoted to the dependence of functional activity on the structure of the metallosurfactants, and the results obtained demonstrate that the nature of both ligand and metal is significant.[14—17] We studied the properties and established a polyfunctional action of complexes based on cationic surfactants with a bicyclic head group, *viz.*, alkylated derivatives of 1,4-diazabicyclo[2.2.2]octane (DABCO) and transition metals (Cu^{2+}, Ni^{2+}, Co^{2+}, La^{3+}).[18—21] As compared to ligands and conventional surfactants, these metallosurfactants demonstrate higher aggregation activity. High solubilizing effect on dyes and pharmaceuticals (nitrofurantoin, griseofulvin, quercetin), biological activity, and the ability to catalyze hydrolysis of organophosphorus ecotoxicants were established.

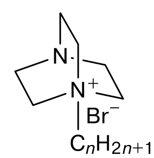

D-*n* (n = 14, 16, 18)

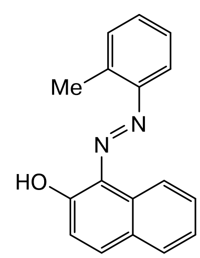

Orange OT

Amphiphilic palladium complexes exhibit not only high biological activity,[22] but also high catalytic activity. In particular, they can act as water-soluble catalysts of Suzuki cross-coupling reaction in water at room temperature.[23,24] These features offer prospects for application of such metallosurfactants in medicine and practical catalysis.

In this work we synthesized a new complex of 1-hexadecyl-4-aza-1-azoniabicyclo[2.2.2]octane bromide (**D-16**) with palladium dichloride [**D-16** • $PdCl_2$]. The ability of the complex to undergo self-association in solutions, its effect on the solubility of a hydrophobic dye (solubilizing

Published in Russian in *Izvestiya Akademii Nauk. Seriya Khimicheskaya,* No. 2, pp. 314—321, February, 2022.

1066-5285/22/7102-0314

action), and intrinsic biological (anitimicrobial, hemolytic, and cytotoxic) activity was studied using a wide range of physicochemical methods.

Experimental

Infrared spectra were recorded on a Bruker Vector 22 FT IR spectrometer in KBr pellets, ^{1}H NMR spectra of solutions in DMSO-d_6 were recorded on a Bruker AVANCE-400 spectrometer operating at 400 MHz with Me_4Si as internal reference. Electronic absorption spectra of solutions in the wavelength range of 190—1100 nm were recorded on a Specord 250 Plus spectrophotometer (Analytik Jena AG, Germany) in thermostatted quartz cells. The optical density (*A*) was measured to an accuracy of ±1%.

The surface tension isotherms at the interface (γ/mN m^{-1}) were obtained by the Du Noüy ring detachment method on a K6 tensiometer (Kruss, Germany). The specific conductivity (χ/μS cm^{-1}) of solutions was measured using an InoLab Cond Level 1 conductivity meter (Germany). Potentiometric measurements were carried out using a bromide-ion selective electrode. The concentration of free bromide ions ([Br^-]/mol L^{-1}) was measured on an I-160MI ionometer using an ELIS-131Br bromide-ion selective electrode. An ESR-10101 electrode was used as reference electrode. The size of aggregates was determined using a Malvern Zetasizer Nano system (United Kingdom) for characterization of nanoparticles. The light scattering angle was 173°. A He—Ne laser (λ = 633 nm) was used as a radiation source. Solubilization of Orange OT was achieved by adding an excess amount of crystalline dye to the metallosurfactant solutions of particular concentration followed by storage of the solutions for 48 h. Spectra of the dye-saturated filtered solutions of the complex were recorded relative to the dye-free metallosurfactant reference solutions of the same concentration. The cell thickness (*l*) was 1.0, 0.5, and 0.1 cm.

The ligand, 1-hexadecyl-4-aza-1-azoniabicyclo[2.2.2]octane bromide (D-16), was obtained by quaternization of DABCO with hexadecyl bromide following a known procedure.[25] Palladium dichloride (99.999%, Alfa Aesar) and the dye 1-(*o*-tolylazo)-2-naphthol (Orange OT, 75%, Aldrich, USA) were used without preliminary purification. Solutions were prepared using water purified with a Direct-Q 5 UV system (Millipore S.A.S. 67120 Molsheim-France) and freshly distilled DMSO (99.8%, Laverna, Russia).

Synthesis of metallosurfactant [D-16 • $PdCl_2$]. To a solution of **D-16** (0.7 g, 0.17 mmol) in water, a solution of $PdCl_2$ (0.29 g, 0.17 mmol) in water (15 mL) heated to 70 °C was added with stirring. The reaction mass was stirred for 30 min. The complex precipitated (Scheme 1) was separated from the solution by centrifugation (15 min, 15000 rpm, 19621 *g*), washed with hot water (6 mL), and dried *in vacuo* on a boiling water bath (50 °C) until constant weight. The yield was 0.85 g (85%). The isolated substance of the composition [**D-16** • $PdCl_2$] was identified by elemental analysis, IR spectroscopy, and ^{1}H NMR spectroscopy. Found (%): C, 44.28; H, 7.64; Br, 12.34; Cl, 10.97; N, 4.07; Pd, 18.23. $C_{22}H_{45}BrCl_2N_2Pd$. Calculated (%): C, 44.42; H, 7.62; Br, 13.43; Cl, 11.94; N, 4.71; Pd, 17.89. IR, ν/cm^{-1}: 2919, 2850, 1468, 1383, 1094, 1055, 812, 720. ^{1}H NMR, δ: 0.87 (t, 3 H, $N^+CH_2CH_2(CH_2)_{13}C\underline{H}_3$, *J* = 6.6 Hz); 1.25 (br.s, 26 H, $N^+CH_2CH_2(C\underline{H}_2)_{13}CH_3$); 1.66 (br.s, 2 H, $CH_2C\underline{H}_2(CH_2)_{13}CH_3$); 3.04 (t, 6 H, $N(CH_2)_3$), *J* = 7.5 Hz); 3.15—3.19 (m, 2 H, $N^+C\underline{H}_2CH_2(CH_2)_{13}CH_3$); 3.27 (t, 6 H, $N^+(CH_2)_3$, *J* = 8.4 Hz). The electronic absorption spectrum of the solution of metallosurfactant in DMSO—water mixture (50 : 50, v/v) exhibits a shoulder in the region of 380—500 nm.

Scheme 1

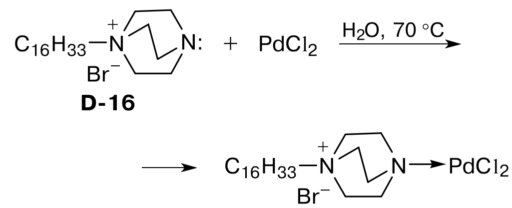

The antimicrobial activity of the test compounds was determined by serial microdilutions in Mueller—Hinton broth for bacterial cultivation and in Sabouraud dextrose broth for fungal pathogens using 96-well plates. Experiments were carried out with the following cultures: Gram-positive bacteria *Staphylococcus aureus* ATCC 6538 P FDA 209P (*Sa*), *Bacillus cereus* ATCC 10702 NCTC 8035 (*Bc*), and *Enterococcus faecalis* ATCC 29212 (*Ef*) and the Gram-negative bacteria *Escherichia coli* ATCC 25922 (*Ec*), *Pseudomonas aeruginosa* ATCC 9027 (*Pa*), and fungi *Trichophyton mentagrophytes var. Gypseum* 1773 (*Tm*), and *Candida albicans* ATCC 10231 (*Ca*). Methicillin-resistant *Staphylococcus aureus* (MRSA) strains were isolated from patients with chronic tonsillitis (MRSA-1) and sinusitis (MRSA-2) in the bacteriological laboratory at the Republican Clinical Hospital (Kazan, Russia). The bacterial load was 3.0 • 10^5 cfu mL^{-1}. The results were recorded every 24 h over a period of 120 h. Bacterial and fungal cultures were incubated at 37 and 25 °C, respectively. The experiments were repeated three times. For better solubility of compounds, 5% DMSO was added to the nutrient medium; no viability loss of the tested strains was detected at this concentration. The minimum inhibitory concentration (MIC) was defined as the lowest concentration of a compound that completely inhibits the growth of a test strain. During the experiments we detected the growth or inhibition of the growth of bacterial or fungal colonies owing to the bacteriostatic or fungistatic action of the tested compounds. To determine the minimum bactericidal concentration or the minimum fungicidal concentration (MBC and MFC, respectively), an aliquot of the bacterial or fungal culture was transferred to Mueller—Hinton agar and incubated at 37 or 25 °C, respectively. The MBC and MFC are the lowest concentrations at which no bacterial or fungal colonies were detected (in other words, the microorganisms were killed with an efficiency of more than 99.9%).[26]

The hemolytic activity of the compounds was estimated by comparing the optical density of a solution containing the test compound and that of blood at 100% hemolysis. A 10% suspension of human erythrocytes was used as an object of investigation. Measurements were carried out using an Invitrologic microplate reader (Russia) at λ = 540 nm.[26] The hemolytic and cytotoxic activity of the complex was studied in the concentration range of 500—0.25 μg mL^{-1}.

The cytotoxic effects of the test compounds on the Chang liver normal human hepatocyte cell line was estimated using the Cytell cell imaging system (GE Health Care Life Science, Sweden) and the Cell Viability Bio application. Fluorescent dyes 4′,6-diamidino-2-phenylindole (DAPI) and propidium iodide used in the experiments were purchased from Sigma. The Chang liver normal human hepatocyte cell line was obtained from the Gamaleya Research Institute of Epidemiology and Microbiology while the WI-38 normal human fetal lung cell line (WI-38 VA 13 subline 2RA) was obtained from Collection of the Institute of Cytology, Russian Academy of Sciences (St. Petersburg, Russia). The cells were cultured in a standard Eagle′s nutrient medium (PanEco Ltd., Russia) and supplemented with 10% fetal calf serum and 1% essential amino acids. The cells ($1 \cdot 10^5$ cell mL^{-1}) were placed into a 96-well plate (Eppendorf), 150 μL of suspension per well, and cultured in a CO_2 incubator at 37 °C. After 24 h, the test compounds pre-diluted in the nutrient medium were added, 150 μL to each well. For better solubility of compounds, 5% DMSO was added to the nutrient medium; no viability loss of the cells was detected at this concentration. The experiments were repeated three times. Intact cells cultured in parallel with the experimental cells were used as a control.[27]

The HC_{50} (concentration that causes 50% hemolysis of human erythrocytes) and IC_{50} (concentration at which a substance exerts half of its maximal inhibitory effect) values were calculated with the IC50 calculator (AAT Bioquest, Inc., USA) used to determine the IC_{50} values from experimental data.[28] Tabulated data include the average values and the standard error.

Results and Discussion

We synthesized a new complex of **D-16** with palladium dichloride [**D-16** • $PdCl_2$]. The composition of the complex was confirmed by IR and ^1H NMR spectroscopies and by elemental analysis. The complex is characterized by a metal : ligand ratio of 1 : 1. The IR spectrum of the complex exhibits a number of absorption bands that are characteristic of **D-16** and originate from vibrations of bicyclic groups in DABCO. An absorption band at 721 cm^{-1} corresponds to rocking vibrations of the long-chain alkyl radical. On going from the ligand to the metallosurfactant the IR band at 1377 cm^{-1} is shifted by 6 cm^{-1}, the band at 1055 cm^{-1} corresponding to stretching vibrations of the C—N bond with participation of the nitrogen atom with the lone electron pair is shifted by 3 cm^{-1}. In addition, a new band characteristic of all complexes based on **D-16** (see Ref. 9) appears at 812 cm^{-1}.

Changes in the IR spectral parameters upon complexation agree with ^1H NMR spectroscopy data for the compound under study. The ^1H NMR spectrum of the metallosurfactant exhibits signals from protons of three CH_2 groups in the bicyclic moiety at the neutral nitrogen atom, one CH_2 group of the long-chain alkyl radical at the nitrogen atom, and three CH_2 groups in the bicyclic moiety at the charged nitrogen atom (at δ 3.04, 3.15—3.19, and 3.27, respectively). They are slightly shifted (by 0.02 ppm) and broadened compared to the ^1H NMR spectrum of the **D-16**. A similar small downfield shift accompanied by broadening of signals and changes in multiplicity is also characteristic of protons of the long-chain alkyl radical (δ 0.87, 1.25, 1.66). These spectral changes are due to the presence of the metal, Pd^{II}, in the structure of the complex [**D-16** • $PdCl_2$] and suggest an electron density redistribution in the surfactant molecule.

The micelle-forming and solubilization properties of the complex [**D-16** • $PdCl_2$] were studied by tensiometry, conductometry, potentiometry, dynamic and electrophoretic light scattering, and spectrophotometry (solubilization of Orange OT dye). To increase the metallosurfactant solubility, the characteristic parameters were measured in a DMSO—water mixture (50 : 50, v/v) at 55 °C.

An increase in the concentration of the metallosurfactant in solutions causes a decrease in the surface tension at air—liquid interfaces (Fig. 1) characteristic of micelle-forming surfactants. The first and second inflection points in the characteristic curve can be associated with the onset of aggregation in the system (critical aggregation concentration, CAC_1) and with the structural rearrangement in the aggregates (CAC_2) (Table 1), respectively.

In Fig. 2, the specific conductivity of solutions of the complex in question is plotted *vs.* its concentration. At low concentrations ($C < CAC_1$), the specific conductivity increases regularly with increasing concentration and then abnormally decreases at $C > CAC_1$. The specific conductivity (χ) of surfactant solutions is mainly determined by nonassociated amphiphile particles, and aggregation at $C > CAC_1$ followed by structural rearrangement at $C > CAC_2$ usually lead to a less pronounced increase in χ with increasing concentration.[29] The decrease in specific conductivity

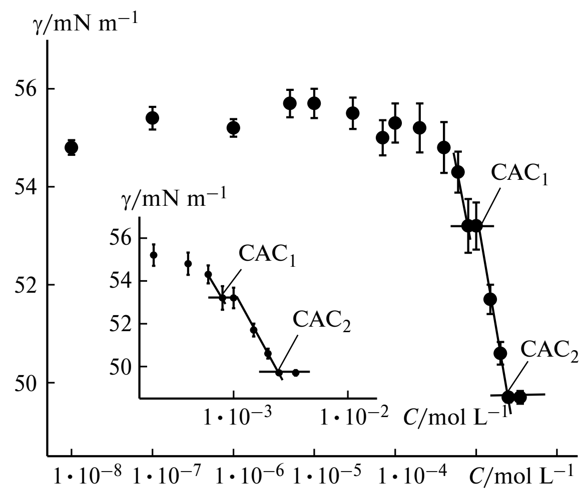

Fig. 1. The surface tension isotherm of solutions of the complex [**D-16** • $PdCl_2$] in DMSO—water mixture (50 : 50, v/v) at 55 °C. Inset: magnified portion of the isotherm in the region corresponding to the onset of surfactant aggregation (CAC_1) and structural rearrangement of aggregates (CAC_2).

Table 1. Critical aggregation concentration of the metal complex [**D-16** • $PdCl_2$] in DMSO—water mixture (50 : 50, v/v) at 55 °C determined by different methods

Parameter	CAC/mmol L^{-1}			
	Tensiometry	Conductometry	Solubilization	Potentiometry
CAC_1	0.8	0.8	0.8	—
CAC_2	2.6	2.5	3.0	2.5

after the aggregation threshold in solutions of the complex can be associated with high cooperativity of self-association of the metallosurfactant in the solutions and with very high ability of aggregates of the Pd^{II} complex to bind counterions (bromide ions). The latter factor seems to play an important role. Supramolecular structures formed in the region of aggregation threshold bind counterions so strongly that the specific conductivity of solutions of the system decreases with increasing concentration rather than slowly increases at $C > CAC_1$, and a maximum appears on the characteristic curve. This interpretation is substantiated by the potentiometrically determined decrease in the concentration of free bromide ions up to $C = CAC_2$. Structural rearrangement of aggregates is followed by an increase in the concentration of free counterions and the specific conductivity of solutions no longer decreases (see Fig. 2).

The ability of metallosurfactants to self-association in water-organic media and structural rearrangements in the system are also confirmed by the results of dynamic and electrophoretic light scattering studies. The hydrodynamic diameter of aggregates (D_H/nm, Fig. 3) was calculated in the spherical approximation (Stokes—Einstein law) and a monomodal size distribution of supramolecular structures was established. The D_H values determined from the number of particles suggest the formation of presumably vesicle-type aggregates 236 nm in size in the region of CAC_1. The possibility for metallosurfactants to form not only micellar, but also vesicle-type aggregates was reported earlier.[30,31] The size of supramolecular structures increases to 415 nm at $C = CAC_2$ and then decreases to 300 nm (compaction) with increasing concentration. The size of aggregates determined with allowance for scattering intensity agrees with these D_H values (Table 2). The zeta-potential (ζ/mV) of the system based on the palladium complex increases from +27 to +54 mV with increasing concentration (see Fig. 3), thus indicating a high stability of the system.[32,33]

Specific features of self-association of the metallosurfactant [**D-16** • $PdCl_2$] in DMSO—water mixture (50 : 50, v/v) also manifest themselves in solubilization of the hydrophobic dye Orange OT. A metallosurfactant-free saturated solution of the dye in the mixed solvent is characterized by high reduced optical density at 495 nm in contrast to aqueous medium where Orange OT is almost insoluble (Fig. 4). This suggests partial dissolution of the chromophore. The introduction of the complex in the pre-aggregation concentration range and an increase in its concentration to $CAC_1 = 0.8$ mmol L^{-1} (region I) leads to up to a threefold increase in A_{495} (Fig. 5). However, at a metallosurfactant concentration of 0.2—0.4 mmol L^{-1}, the intensity of the long-wavelength shoulder of the dye

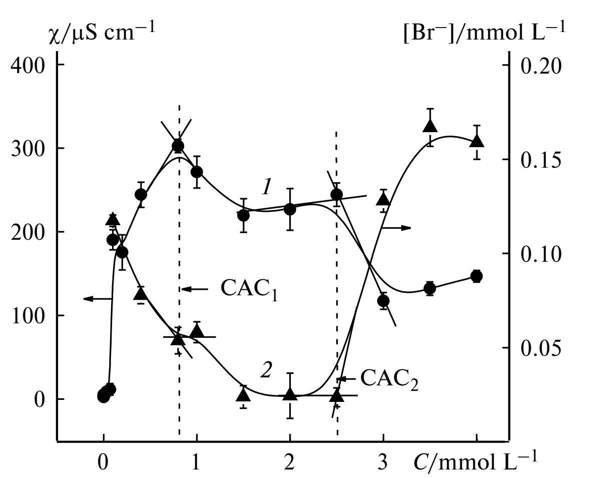

Fig. 2. Specific conductivity (*1*) and concentration of free bromide ions (*2*) in solutions of the complex [**D-16** • $PdCl_2$] in DMSO— water mixture (50 : 50, v/v) at 55 °C plotted *vs*. concentration of the complex.

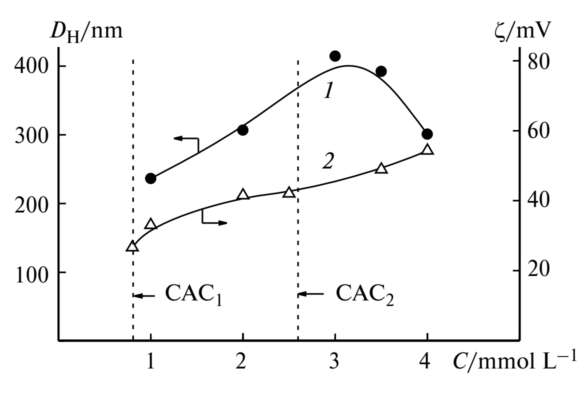

Fig. 3. Hydrodynamic diameter of aggregates of the complex [**D-16** • $PdCl_2$] in DMSO—water mixture (50 : 50, v/v) determined from the number of particles (*1*) and the zeta-potential (ζ) of the system (*2*) plotted *vs*. concentration of the complex at 55 °C.

Table 2. Hydrodynamic diameters (D_H) of the complex [**D-16** • $PdCl_2$] determined with allowance for scattering intensity and the polydispersity indices (PdI) at different surfactant concentrations in DMSO—water mixture (50 : 50, v/v) at 55 °C

C/mmol L^{-1}	D_H (from intensity)/nm	PdI
1.0	237	0.388
2.0	307	0.086
3.0	416	0.118
3.5	393	0.100
4.0	300	0.255

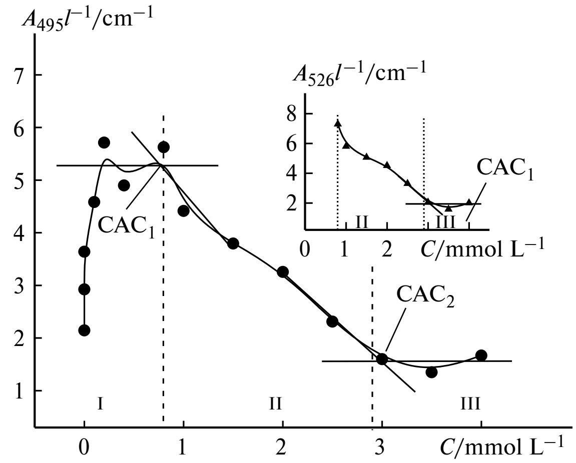

Fig. 5. Reduced optical density in the absorption spectra of Orange OT at 495 nm (regions I and II) and that of absorption bands with maxima at 495—546 nm (region III) of solutions of the complex [**D-16** • $PdCl_2$] plotted *vs.* its concentration in DMSO—water mixture (50 : 50, v/v) at 55 °C. Inset: plot of reduced optical density at 526 nm (region II) and that of absorption bands with maxima at 495—546 nm (region III) *vs.* concentration of the complex [**D-16** • $PdCl_2$] in DMSO—water mixture (50 : 50, v/v) at 55 °C.

band increases and a maximum at 526 nm appears (see Fig. 4). Note that at C = CAC$_1$, the parameter A_{526} takes the maximum value and a further increase in the surfactant concentration from CAC$_1$ to CAC$_2$ (region II) is accompanied by a decrease in both A_{495} and A_{526} (see Fig. 5). At C > CAC$_2$ (3 mmol L^{-1}), the absorption intensity in region III almost no longer decreases and the band at 526 nm is shifted to 546 nm (see Fig. 4).

The position and shape of the most intense absorption band of the Orange OT dye in the visible region depends strongly on the microenvironment. In polar solvents (methanol—water mixture (50 : 50, v/v) and methanol) the main band has a maximum at 495 nm and a characteristic shoulder in the long-wavelength region.[34] In aqueous micellar solutions the band maximum of the solubilized dye was observed at 495 nm (for, *e.g.*, conventional cationic surfactants[34] or a nonionic surfactant[35]), at 523 nm (anionic surfactant[36]) or simultaneously at 499 and 521 nm (anionic surfactant[35]). The supramolecular systems under study demonstrate all three variants depending on the content of metallosurfactant in solutions, *viz.*, an individual maximum at 495 nm and a shoulder in the longer-wavelength region (initial portion of region I), two maxima at 495 and 526 nm (final portion of region I), and a maximum at 526 nm with a shoulder in the shorter-wavelength region (region II) (see Fig. 4). Different shapes of the spectral band and positions of its maximum are indicative of significant changes in the microenvironment of the dye on going from the solution bulk to the pre-vesicle-type (region I) and then vesicle-type aggregates (region II). Binding of Orange OT to the pre-vesicle-type associates characterized by low association number and weakly pronounced region of low polarity gives rise to the accumulation of the dye in the region with lower dielectric permittivity (ε) as compared to the bulk phase (it equals 64.4 at 55 °C according to calculations[37] using the data for aqueous DMSO solution with a DMSO mole fraction of 0.2). At C > CAC$_1$, the onset of aggregation (with the most probable formation of linear aggregates) is followed by a more pronounced transfer of the dye to vesicles, which is driven by hydrophobic and ion-dipole interactions, and its concentration in the near-boundary layer of the low-polarity region adjacent to the palladium-containing outer layer of the surfactant head groups. A sharper decrease in the intensity of the peak at 526 nm with increasing concentration at C > CAC$_1$ (region II, see Fig. 5) suggests a decrease in the content of the aza dye in the vesicles, probably, owing to its partial decomposition in the metal-

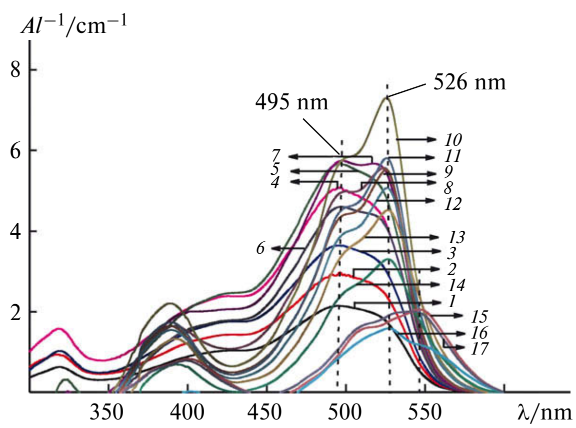

Fig. 4. Absorption spectra of Orange OT in dye-saturated solutions of the complex [**D-16** • $PdCl_2$] in DMSO—water mixture (50 : 50, v/v) at a complex concentration of 0 (*1*), 0.0001 (*2*), 0.001 (*3*), 0.03 (*4*), 0.07 (*5*), 0.1 (*6*), 0.2 (*7*), 0.4 (*8*), 0.6 (*9*), 0.8 (*10*), 1.0 (*11*), 1.5 (*12*), 2.0 (*13*), 2.5 (*14*), 3.0 (*15*), 3.5 (*16*), and 4.0 mmol L^{-1} (*17*); 55 °C; Al^{-1} is the reduced optical density (*l* is the optical path length, cell thickness).

Table 3. Anitimicrobial activity of the complex, ligand, and test pharmaceuticals

Compound	*Sa*	*Bc*	*Ef*	*Ec*	*Pa*	*Tm*	*Ca*
Bacteriostatic and fungistatic activity, MIC/μg mL^{-1}							
[**D-16** · $PdCl_2$]	0.9±0.07	1.9±0.1	0.9±0.07	15.6±1.3	250±18	—	7.8±0.6
D-16*	0.3	1.9	—	6.3	500	62.5	3.1
Norfloxacin	2.4±0.2	7.8±0.6	2.4±0.2	1.5±0.1	3.9±0.2	—	—
Ketoconazole	—	—	—	—	—	3.9±0.3	3.9±0.2
Bactericidal and fungicidal activity, MBC or MFC/μg mL^{-1}							
[**D-16** · $PdCl_2$]	0.9±0.07	125±10	3.9±0.2	62.5±5.4	—	—	15.6±1.3
D-16*	5.0	500	—	>500	>500	500	50
Norfloxacin	2.4±0.2	7.8±0.6	2.4±0.2	7.8±0.6	15.6±1.3	—	—
Ketoconazole	—	—	—	—	—	3.9±0.2	3.9±0.2

* Data taken from Ref. 40.

containing medium.[38,39] Structural rearrangement of aggregates at $C > CAC_2$ is accompanied by a shift of the band at 526 nm toward the long-wavelength region. This seems to be due to significant changes in the parameters of the system (concentration of free bromide ions, specific conductivity (see Fig. 2), morphology, microviscosity, micropolarity, *etc*.) and to the occurrence of processes involving the dye. We studied the anitimicrobial activity of the palladium complex against Gram-positive and Gram-negative bacteria and fungi. It was established that the metallosurfactant can simultaneously exhibit antibacterial and fungicidal activity. The MIC of the complex against *Staphylococcus aureus*, *Bacillus cereus*, and *Enterococcus faecalis* is 2.7, 4.1, and 2.7 times lower compared to norfloxacin (Table 3). The bactericidal activity of the complex against *Staphylococcus aureus* is also 2.7 and 5.6 times higher compared to the test compound (norfloxacin) and **D-16**, respectively. The fungicidal activity of the complex against *Candida albicans* is 3.2 times higher compared to **D-16** (see Table 3). Thus, the complex under study demonstrates high anitimicrobial activity which in some cases is higher than that of norfloxacin and **D-16**.

Table 4. Anitimicrobial activity of metal complexes toward methicillin-resistant *Staphylococcus aureus* strains

Compound	*Sa*	MRSA-1	MRSA-2
Bacteriostatic and fungistatic activity, MIC/μg mL^{-1}			
[**D-16** · $PdCl_2$]	0.9±0.08	1.9±0.1	0.9±0.07
Amoxicillin	0.3±0.02	31.3±2.6	31.3±2.5
Ciprofloxacin	0.5±0.04	125±11	0.9±0.07
Bactericidal activity, MBC/ μg mL^{-1}			
[**D-16** · $PdCl_2$]	0.9±0.07	15.6±1.3	15.6±1.2
Amoxicillin	0.9±0.06	31.3±2.5	31.3±2.7
Ciprofloxacin	0.5±0.03	250±19	0.9±0.07

In addition, the complex exhibits high antibacterial activity against the methicillin-resistant strains *Staphylococcus aureus* (MRSA) isolated from patients with chronic tonsillitis (MRSA-1) and sinusitis (MRSA-2) (Table 4). The MIC of the metallosurfactant against MRSA-1 is 16 and 66 times lower than that of amoxicillin and ciprofloxacin, respectively. The bacteriostatic activity of the complex against MRSA-2 is 35 times higher than that of amoxicillin. The bactericidal activity of the metal complex is also high, *viz*., its MBC against MRSA-1 is two and sixteen times lower than that of amoxicillin and ciprofloxacin, respectively.

Table 5 presents the data on the cytotoxic effect of the complex against human erythrocytes (hemolytic activity). The HC_{50} value is 102 μg mL^{-1}, being more than two orders of magnitude higher than the MIC of the metallosurfactant against *Staphylococcus aureus* (selectivity index IS = HC_{50}/MIC(*Sa*)). This points to high selectivity of antimicrobial action of the metal complex since its IS value much exceeds that of traditional cationic surfactant hexadecyltrimethylammonium bromide (HTAB) (see Table 5).

The cytotoxicity of the complex on the WI-38 normal human fetal lung cell line and on the Chang liver normal human hepatocyte cell line also characterizes its high selectivity against *Staphylococcus aureus* (IS = 93). Besides, the cytotoxicity (IC_{50}) of the complex on Chang liver normal human hepatocyte cells is 28 times lower compared to doxorubicin and two times lower compared to tamoxifen (see Table 5).

Summing up, we revealed the formation of large (presumably, vesicle-type) aggregates in solutions of the new complex of 1-hexadecyl-4-aza-1-azoniabicyclo-[2.2.2]octane bromide with palladium dichloride in DMSO—water mixture. It was also established that the aggregation parameters of the system depend on the concentration of the complex in the solution. At low concentrations (0.8 mmol L^{-1}), about 240-nm aggregates are formed. At C = 2.5—3.0 mmol L^{-1}, a structural rear-

Table 5. Hemolytic activity (HC_{50}) and cytotoxic effect of the complex on the WI-38 normal human fetal lung cell line and the Chang liver normal human hepatocyte cell line (IC_{50}), and the selectivity of antimicrobial action of the metallosurfactant (IS)

Compound	Hemolytic activity		Cytotoxic effect		
	HC_{50}/μg mL^{-1}	IS = HC_{50}/MIC(*Sa*)	Cell line	IC_{50}/μg mL^{-1}	IS = IC_{50}/MIC(*Sa*)
[**D-16** · $PdCl_2$]	102	113	WI38	83.6	93.0
[**D-16** · $PdCl_2$]	—	—	Chang liver	84.0	93.3
HTAB	1.82*	3.64**	—	—	—
Doxorubicin***	—	—	Chang liver	3.0	—
Tamoxifen***	—	—	Chang liver	42.1	—

* Data taken from Ref. 41.

** MIC(*Sa*) = 0.5 μg mL^{-1}.

*** Data taken from Ref. 26.

rangement of the aggregates occurs and their size increases to 420 nm. We also studied the solubilizing and biological activity of the metallosurfactant. The complex exhibits a concentration-dependent solubilizing action on hydrophobic dye Orange OT, high anitimicrobial activity, and low hemolytic activity. In addition, it is characterized by much lower cytotoxic effect on the WI-38 normal human fetal lung cell line and on the Chang liver normal human hepatocyte cell line compared to doxorubicin and tamoxifen. These data demonstrate a high potential of the complex for biomedical applications and its ability to act as a new anitimicrobial drug.

This work was financially supported by the Russian Science Foundation (Project No. 19-73-30012).

No human or animal subjects were used in this research.

The authors declare no competing interests.

References

1. G. Kaur, P. Garg, B. Kaur, G. R. Chaudhary, S. Kumar, N. Dilbaghi, P. A. Hassan, S. L. Gawali, *Soft Matter*, 2018, **14**, 5306; DOI: 10.1039/c8sm00535d.
2. N. Kaur, S. Kaur, G. Kaur, A. Bhalla, S. Srinivasan, G. R. Chaudhary, *J. Mater. Chem. A*, 2019, **7**, 17306; DOI: 10.1039/c9ta05441c.
3. B. Kaur, G. R. Chaudhary, G. Kaur, *J. Mater. Chem. B*, 2019, **7**, 3679; DOI: 10.1039/c9tb00607a.
4. R. F. P. Pereira, A. J. M. Valente, H. D. Burrows, V. de Zea Bermudez, R. A. Carvalho, R. A. E. Castro, *RSC Adv.*, 2013, **3**, 1420; DOI: 10.1039/c2ra21906a.
5. P. A. Demakov, A. S. Romanov, D. G. Samsonenko, D. N. Dybtsev, V. P. Fedin, *Russ. Chem. Bull.*, 2020, **69**, 1511; DOI: 10.1007/s11172-020-2930-4.
6. G. Kaur, V. Dogra, R. Kumar, S. Kumar, K. Singh, *J. Biomol. Struct. Dyn.*, 2019, **37**, 892; DOI: 10.1080/07391102.2018.1442251.
7. S. K. Mehta, R. Kaur, G. R. Chaudhary, *Colloids Surf. A: Physicochem. Eng. Aspects*, 2012, **403**, 103; DOI: 10.1016/j.colsurfa.2012.03.062.
8. S. M. Tawfik, M. F. Zaky, *J. Surfactants Deterg.*, 2015, **18**, 863; DOI: 10.1007/s11743-015-1700-z.
9. E. P. Zhiltsova, M. R. Ibatullina, S. S. Lukashenko, F. G. Valeeva, T. N. Pashirova, M. P. Kutyreva, L. Ya. Zakharova, *Colloid J.*, 2017, **79**, 621; DOI: 10.1134/S1061933X17050179.
10. G. La Sorella, G. Strukul, A. Scarso, *Green Chem.*, 2015, **17**, 644; DOI: 10.1039/c4gc01368a.
11. G. Kaur, S. Kumar, N. Dilbaghi, G. Bhanjana, S. K. Guru, S. Bhushan, S. Jaglan, P.A. Hassan, V. K. Aswal, *Phys. Chem. Chem. Phys.*, 2016, **18**, 23961; DOI: 10.1039/c6cp03070j.
12. A. B. Mirgorodskaya, R. A. Kushnazarova, F. G. Valeeva, S. S. Lukashenko, A. A. Tyryshkina, L. Ya. Zakharova, O. G. Sinyashin, *Mendeleev Commun.*, 2021, **31**, 323; DOI: 10.1016/j.mencom.2021.05.014.
13. M. R. Ibatullina, E. P. Zhil´tsova, S. S. Lukashenko, V. I. Kovalenko, I. I. Vandyukova, M. P. Kutyreva, L. Ya. Zakharova, *Russ. Chem. Bull.*, 2019, **68**, 424; DOI: 10.1007/s11172-019-2403-9.
14. K. K Ghosh, B. Gupta, S. Bhattacharya, *Curr. Organocatal.*, 2016, **3**, 6; DOI: 10.2174/2213337202666150713174927.
15. W. A. Wani, S. Prashar, S. Shreaz, S. Gómez-Ruiz, *Coord. Chem. Rev.*, 2016, **312**, 67; DOI: 10.1016/j.ccr.2016.01.001.
16. R. Kaur, S. K. Mehta, *Coord. Chem. Rev.*, 2014, **262**, 37; DOI: 10.1016/j.ccr.2013.12.014.
17. S. M. Magami, Z. N. Garba, M. B. Ibrahim, *J. Mater. Sci. Chem. Eng.*, 2015, **3**, 22; DOI: 10.4236/msce.2015.310004.
18. E. P. Zhil´tsova, M. R. Ibatullina, S. S. Lukashenko, M. P. Kutyreva, M. M. Anuar, V. I. Kovalenko, L. Ya. Zakharova, *Russ. J. Gen. Chem.*, 2017, **87**, 2620; DOI: 10.1134/S1070363217110172.
19. E. P. Zhiltsova, T. N. Pashirova, M. R. Ibatullina, S. S. Lukashenko, A. T. Gubaidullin, D. R. Islamov, O. N. Kataeva, M. P. Kutyreva, L. Ya. Zakharova, *Phys. Chem. Chem. Phys.*, 2018, **20**, 12688; DOI: 10.1039/c8cp01954a.
20. E. P. Zhiltsova, M. R. Ibatullina, S. S. Lukashenko, M. P. Kutyreva, L. Ya. Zakharova, *J. Mol. Liq.*, 2018, **249**, 716; DOI: 10.1016/j.molliq.2017.11.091.
21. E. P. Zhil´tsova, M. R. Ibatullina, S. S. Lukashenko, I. R. Nizameev, M. K. Kadirov, L. Ya. Zakharova, *Kinet. Catal.*, 2020, **61**, 269; DOI: 10.1134/S0023158420010140.
22. G. Kaur, S. Kumar, N. Dilbaghi, B. Kaur, R. Kant, S. K. Guru, S. Bhushan, S. Jaglan, *Dalton Trans.*, 2016, **45**, 6582; DOI: 10.1039/c6dt00312e.
23. N. Kaur, G. Kaur, A. Bhalla, J. S. Dhau, G. R. Chaudhary, *Green Chem.*, 2018, **20**, 1506; DOI: 10.1039/c7gc03877a.
24. P. Qiu, J.Y. Zhao, X. Shi, X.H. Duan, *New J. Chem.*, 2016, **40**, 6568; DOI: 10.1039/c6nj00377j.

25. T. N. Pashirova, E. P. Zhil´tsova, R. R. Kashapov, S. S. Lukashenko, A. I. Litvinov, M. K. Kadirov, L. Ya. Zakharova, A. I. Konovalov, *Russ. Chem. Bull.*, 2010, **59**, 1745.
26. A. D. Voloshina, S. K. Gumerova, A. S. Sapunova, N. V. Kulik, A. B. Mirgorodskaya, A. A. Kotenko, T. M. Prokopyeva, V. A. Mikhailov, L. Ya. Zakharova, O. G. Sinyashin, *Biochim. Biophys. Acta*, *Gen. Subj.*, 2020, **1864**, 129728; DOI: 10.1016/j.bbagen.2020.129728.
27. A. D. Voloshina, A. S. Sapunova, N. V. Kulik, M. G. Belenok, I. Yu. Strobykina, A. P. Lyubina, S. K. Gumerova, V. E. Kataev, *Bioorg. Med. Chem.*, 2021, **32**, 115974; DOI: 10.1016/j.bmc.2020.115974.
28. *AAT Bioquest*, *Inc.*, 4 Jun. 2021; https://www.aatbio.com/tools/ic50-calculator.
29. M. R. Ibatullina, E. P. Zhil´tsova, S. S. Lukashenko, V. I. Kovalenko, I. I. Vandyukova, M. P. Kutyreva, L. Ya. Zakharova, *Russ. Chem. Bull.*, 2019, **68**, 424; DOI: 10.1007/s11172-019-2403-9.
30. G. A. Koutsantonis, G. L. Nealon, C. E. Buckley, M. Paskevicius, L. Douce, J. M. Harrowfield, A. W. McDowall, *Langmuir*, 2007, **23**, 11986; DOI: 10.1021/la701283b.
31. M. R. Ibatullina, E. P. Zhil´tsova, S. S. Lukashenko, A. D. Voloshina, A. S. Sapunova, O. A. Lenina, I. R. Nizameev, M. P. Kutyreva, L. Ya. Zakharova, *Russ. J. Gen. Chem.*, 2018, **88**, 2359; DOI: 10.1134/S107036321811018X.
32. S. Nehru, S. Veeralakshmi, S. Arunachalam, *New J. Chem.*, 2017, **41**, 13830; DOI: 10.1039/c7nj02698f.
33. In *Advances in Nanomedicine for the Delivery of Therapeutic Nucleic Acids*, Eds S. Nimesh, R. Chandra, N. Gupta, Elsevier Ltd, Oxford, UK, 2017, p. 43; DOI: 10.1016/B978-0-08-100557-6.00003-1.
34. S. Padasala, K. Kuperkar, P. Bahadur, *Coloration Technol.*, 2016, **132**, 217; DOI: 10.1111/cote.12208.
35. H. Schott, *J. Phys. Chem.*, 1966, **70**, 2966; DOI: 10.1021/j100881a041.
36. J. R. McElhanon, T. Zifer, S. R. Kline, D. R. Wheeler, D. A. Loy, G. M. Jamison, T. M. Long, K. Rahimian, B. A. Simmons, *Langmuir*, 2005, **21**, 3259; DOI: 10.1021/la047074z.
37. E. S. Verstakov, S. A. Korobkova, T. A. Nosaeva, *Russ. J. Phys. Chem. A*, 2020, **94**, 738; DOI: 10.1134/S003602442004024X.
38. F. Duarte, F. J. Maldonado-Hódar, A. F. Pérez-Cadenas, L. M. Madeira, *Appl. Catal. B*, 2009, **85**, 139; DOI: 10.1016/j.apcatb.2008.07.006.
39. N. Ezzatahmadi, T. Bao, H. Liu, G. J. Millar, G. A. Ayoko, J. Zhu, R. Zhu, X. Liang, H. He, Y. Xi, *RSC Adv.*, 2018, **8**, 7687; DOI: 10.1039/c7ra13348k.
40. E. P. Zhil´tsova, T. N. Pashirova, R. R. Kashapov, N. K. Gaisin, O. I. Gnezdilov, S. S. Lukashenko, A. D. Voloshina, N. V. Kulik, V. V. Zobov, L. Ya. Zakharova, A. I. Konovalov, *Russ. Chem. Bull.*, 2012, **61**, 113.
41. N. Joondan, S. Jhaumeer-Laulloo, P. Caumul, M. Akerman, *J. Phys. Org. Chem.* 2017, **30**, e3675; DOI: 10.1002/poc.3675.

Received June 24, 2021;
in revised form August 2, 2021;
accepted August 18, 2021